Molecular Neurobiology
https://doi.org/10.1007/s12035-018-1152-3

Proliferative Glioblastoma Cancer Cells Exhibit Persisting Temporal Control of Metabolism and Display Differential Temporal Drug Susceptibility in Chemotherapy

Paula M. Wagner[1,2] · Lucas G. Sosa Alderete[1,2,3] · Lucas D. Gorné[4,5] · Virginia Gaveglio[6] · Gabriela Salvador[6] · Susana Pasquaré[6] · Mario E. Guido[1,2]

Received: 1 December 2017 / Accepted: 24 May 2018

Abstract

Even in immortalized cell lines, circadian clocks regulate physiological processes in a time-dependent manner, driving transcriptional and metabolic rhythms, the latter being able to persist without transcription. Circadian rhythm disruptions in modern life (shiftwork, jetlag, etc.) may lead to higher cancer risk. Here, we investigated whether the human glioblastoma T98G cells maintained quiescent or under proliferation keep a functional clock and whether cells display differential time responses to bortezomib chemotherapy. In arrested cultures, mRNAs for clock (*Per1*, *Rev-erbα*) and glycerophospholipid (GPL)-synthesizing enzyme genes, ^{32}P-GPL labeling, and enzyme activities exhibited circadian rhythmicity; oscillations were also found in the redox state/peroxiredoxin oxidation. In proliferating cells, rhythms of gene expression were lost or their periodicity shortened whereas the redox and GPL metabolisms continued to fluctuate with a similar periodicity as under arrest. Cell viability significantly changed over time after bortezomib treatment; however, this rhythmicity and the redox cycles were altered after *Bmal1* knockdown, indicating cross-talk between the transcriptional and the metabolic oscillators. An intrinsic metabolic clock continues to function in proliferating cells, controlling diverse metabolisms and highlighting differential states of tumor suitability for more efficient, time-dependent chemotherapy when the redox state is high and GPL metabolism low.

Keywords Circadian rhythm · Tumor cell · Glioblastoma · Clock gene · Glycerophospholipid metabolism · Redox state

Introduction

In mammals, the circadian timing system generates periodic oscillations in many physiological processes and behaviors, allowing the organism to anticipate and adapt to daily environmental changes and thus be in synchrony with the solar cycle. Circadian clocks are present in most tissues examined and even in immortalized cell lines and primary cell cultures

Paula M. Wagner and Lucas G. Sosa Alderete contributed equally to this work.

Electronic supplementary material The online version of this article (https://doi.org/10.1007/s12035-018-1152-3) contains supplementary material, which is available to authorized users.

✉ Mario E. Guido
mguido@fcq.unc.edu.ar

[1] CIQUIBIC-CONICET, Departamento de Química Biológica, Facultad de Ciencias Químicas, Universidad Nacional de Córdoba, Haya de la Torre s/n, Ciudad Universitaria, 5000 Córdoba, Argentina

[2] Departamento de Química Biológica "Ranwel Caputto", Facultad de Ciencias Químicas, Universidad Nacional de Córdoba, 5000 Córdoba, Argentina

[3] Present address: Department of Molecular Biology, UNRC, CONICET, Río Cuarto, Argentina

[4] Facultad de Ciencias Exactas Físicas y Naturales, Universidad Nacional de Córdoba, Córdoba, Argentina

[5] Consejo Nacional de Investigaciones Científicas y Técnicas, CONICET, Instituto Multidisciplinario de Biología Vegetal (IMBiV), Córdoba, Argentina

[6] Departamento de Biología, Bioquímica y Farmacia, Instituto de Investigaciones Bioquímicas de Bahía Blanca (INIBIBB, UNS-CONICET), Universidad Nacional del Sur, 8000 Bahía Blanca, Argentina

Published online: 07 June 2018

displaying self-sustained rhythms in gene expression and metabolic activities [1–4]. At the molecular level, the clock is controlled by a transcriptional/translational feedback circuitry involving a set of so-called clock genes such as *Clock, Bmal1, Periods (Per)*, and *Cryptochromes (Cry)*, among others, encoding for the corresponding clock proteins acting as regulatory transcription factors (activators or repressors) able to generate rhythms of clock gene and clock-controlled gene expression under a circadian base [5]. Through their rhythmic transcription, circadian clock genes regulate the metabolism and respiration of cells, therefore becoming very important regulators of the cell division cycle [6]. Loss of clock gene function or misalignment of circadian rhythms may therefore lead to diverse metabolic disorders (obesity, diabetes, hyperlipidemia, etc.) [7] and higher risk of cancer by inducing malignant cell growth and tumor development [6].

Carcinogenesis is a process resulting in the accumulation of genetic alterations primarily in genes involved in the regulation of signaling pathways relevant to the regulation of cell growth and division (reviewed in [8]). Characteristics typical of neoplastic processes include sustained proliferative activation, growth suppressor evasion, cell death resistance, replicative immortality, induction of angiogenesis, and invasiveness and metastasis, all of which are based on genome instability and inflammation. In this context, knowledge at the molecular level of circadian biology can contribute significantly to the understanding and potential treatment of human pathologies, in particular cancer and metabolic and behavioral disorders [6, 9]. Moreover, recent transcriptomic, proteomic, and metabolomic studies in mammalian tissues have shown a robust crosslink between the circadian clock and cellular metabolism in general and glycerophospholipid (GPL) homeostasis and metabolism in particular [10–13].

In addition, a redox/metabolic clock that drives peroxiredoxin (PRX) oxidation cycles has recently been reported to operate even in the absence of transcription and shown to be highly conserved through evolution and present in all different kingdoms of life [14, 15]. On the basis of this new evidence, it can be inferred that there is an intrinsic clock at the cellular level, comprising the transcriptional clock and metabolic oscillators that temporally control a plethora of cellular processes. GPLs constitute a fundamental group of lipids with important roles as structural components of all biological membranes and key cellular components involved in cell signaling, energy balance, vesicular transport, cell division, apoptosis, and cell-to-cell communication [16, 17]. Phosphatidylcholine (PC) and phosphatidylethanolamine (PE) are the most abundant GPLs present in all eukaryotic cells; they are first synthesized from glycerol-3-phosphate via a de novo pathway described by Kennedy and Weiss [17, 18] and subsequently remodeled by the Lands Cycle, involving the sequential activity of phospholipases A (PLA) and lysophospholipid acyltransferases (LPLAT) [19, 20]. For PC biosynthesis, the Kennedy pathway involves three enzymatic steps catalyzed by choline kinase (ChoK), CTP/phosphocholine cytidylyltranferase (CCT), and CDP-choline/1,2-diacylglycerol choline phosphotransferase (CPT) in which CCT activity is considered the rate-limiting and regulatory step under most metabolic conditions [21]. Nevertheless, it has been demonstrated that the availability of diacylglycerol (DAG) and regulation of ChoK also influence PC biosynthesis [22–24]. In most mammals, there are two genes encoding for ChoK: *Chka* codes for ChoKα1/2 and *Chkb* codes for ChoKβ [25, 26]. Mice lacking *ChoKα* die early in embryogenesis [25, 26], whereas ChoK overexpression has been implicated in human carcinogenic processes [25, 26]. In addition, *ChoKα* expression and/or activity are subject to circadian control in both cultured fibroblasts and mice liver after synchronization [3, 4, 27]. In mammalian cells, PE is mainly de novo synthesized from the CDP-ethanolamine Kennedy pathway in which ethanolamine (Etn) is phosphorylated to Etn-P by the Etn kinase (EK) and then converted to CDP-Etn by CTP/phosphoethanolamine cytidylyltranferase (*Pcyt2*). In the last step, CDP-Etn is transferred to DAG to produce PE by the CDP-Etn/1,2-diacylglycerol ethanolamine phosphotransferase (EPT). Pcyt2 is the main regulatory enzyme in the de novo biosynthesis of PE (for a review, see [28]). In mammals, the disruption of genes encoding GPL biosynthetic enzymes has severe physiological consequences during development and can be lethal [25, 26].We have previously reported that de novo synthesis of whole GPLs in different cell types from mammalian and non-mammalian vertebrates is controlled by a circadian clock, as observed in chicken retinal neurons in vivo or in vitro [29–31], in the liver of mice synchronized to light-dark cycles [4], as well as in quiescent murine fibroblasts after synchronization by a serum shock [3, 32]. Furthermore, the biosynthesis of membrane GPLs including PC and PE is of crucial significance for cell growth and progression through the cell cycle, whereas deregulated proliferation is a hallmark of cancer cells [8]. Although circadian clocks influence the cell division cycle through complex regulatory circuits, deregulation of core clock gene expression and loss of circadian homeostasis may promote cancer development [6, 33]. At present, little is known about the temporal regulation of GPL biosynthesis in immortalized tumor cells. We therefore investigated whether human glioblastoma T98G cells subject to proliferation in the presence of serum or maintained quiescent (arrested) in a serum-free medium retain a functional clock capable of regulating gene expression at the molecular level and redox and GPL metabolism under a circadian base. To this end, we first examined the expression of clock core genes (*Per1* and *Rev-erbα*) and GPL-synthesizing enzyme genes (*ChoKα* and *Pcyt-2)* for PC and PE biosynthetic pathways, respectively, in proliferating and quiescent cells at different times after dexamethasone (DEX, 100 nM) synchronization.

We also assessed whether redox metabolism (redox state and peroxiredoxin oxidation cycles), the metabolic labeling of ^{32}P-GPLs, and the activities of GPL-synthesizing enzyme phosphatidate phosphohydrolase (PAP) and LPLATs were temporally regulated in synchronized T98G cells after DEX synchronization under both proliferative conditions. We further assessed the susceptibility of proliferating cells over time to treatment with the proteasome inhibitor bortezomib, a known chemotherapeutic agent. Lastly, we investigated the role of the transcriptional clock in redox cycle rhythms and chemotherapeutic susceptibility in proliferating cells in which *Bmal1* expression was knocked-down by CRISPR/cas9 technology.

Results

Characterization of T98G Cell Culture Conditions

T98G glioblastoma cells display typical cancer cell characteristics and are thus subject to continuous proliferation, as a result of which no inhibition by contact is observed when cells are maintained in culture. One round of division along the cell cycle takes close to 24–28 h.

To investigate the temporal regulation of GPL synthesis, redox metabolism and expression of clock and clock-controlled genes in T98G cells, we first characterized the experimental culture conditions in relation to proliferation levels. To this end, cells grown to 50% of confluence in 10% fetal bovine serum (FBS)-Dulbecco's modified Eagle's medium (DMEM) were synchronized with a 20-min 100 nM DEX shock and then maintained in the presence of a 5% serum medium (proliferative) or in an FBS-free medium (arrested) to achieve quiescence for 24 h. Irrespective of the cell cycle itself, a synchronization protocol is essential to adjust individual cells within the whole culture population to the same phase. We examined whether cells undergo a significant rate of cell division after DEX synchronization under both FBS conditions. We found by flow cytometry that within the first 24 h, most cells in this serum-free state were arrested at the G_0/G_1 phases (~ 71–80%) while < 12–17% of cells reached the G_2/M and S phases (Supplementary Fig. 1a). The distribution of cell populations throughout the cell cycle remained constant at all times examined. These two major features—the basal proliferative condition and synchronization by an external factor—make T98G cell cultures an interesting oscillator model for circadian studies, in a cancer context, regardless of cell division and systemic influences from the brain's master clock. At times after at least 8 h of DEX treatment, ~ 60% of cells maintained in the presence of FBS after synchronization were arrested at the G_0/G_1 phases and ~ 30% at the G_2/M and S phases (Supplementary Fig. 1a). The distribution of cell populations throughout the cell cycle in the presence of FBS medium remained constant at most times examined up to 48 h, with an average of ~ 35% of cells in the G_2/M and S phases. On the contrary, at time 0 with no DEX treatment and during the first hour after treatment, cells exhibited the highest percentage at phase S + G_2/M (50–65%) and the lowest for G_o/G_1 (30–40%) as compared with DEX-treated cells at longer times (Supplementary Fig. 1a, b). Based on these observations, it can be inferred that once synchronized, cells from the two conditions (proliferative and arrested) represent different proliferative situations, making them suitable for circadian studies. In addition, when the molecular clock was perturbed in proliferating T98G cells after transfection with PX459-*Bmal1* plasmid in order to knock-down *Bmal1* expression (Supplementary Fig. 1a, c, d), there was a higher percentage of arrested cells (77%) in the G_0/G_1 phases than in the controls (61%).

Temporal Regulation of Clock Gene Expression in T98G Cells Under Different Proliferation Conditions

T98G cells synchronized with a brief DEX shock and maintained arrested in an FBS-free medium displayed a significant temporal variation in mRNA levels for the clock genes *Per1* and *Rev-erbα* along the 48 h examined, with markedly different profiles of expression (Supplementary Fig. 1b) and a periodicity according to a COSINOR/RAIN analysis ranging from 24 to 28 h (Table 1). It is noteworthy that *Bmal1* was highly expressed at time 0 and 24 h after synchronization and lowest levels were seen at 16 h (data not shown), whereas *Per1* and *Rev-erbα* transcripts exhibited patterns of expression in total antiphase with *Bmal1* mRNA (Supplementary Fig. 1b). In fact, highest levels of mRNA for *Per1* and *Rev-erbα* were observed around 16 h after synchronization. The statistical analysis revealed a significant time effect for the two transcripts assessed: mRNA levels for *Per1* and *Rev-erbα* at 16 h were higher than those at 0–8 and 24–30 h.

Although clock gene expression in proliferating T98G cells after DEX synchronization also showed temporal fluctuations in the three clock genes investigated (Supplementary Fig. 1b), the circadian rhythmicity was lost for *Rev-erbα* mRNAs and for *Per1* the period was shortened to 16 h according to the periodic analysis (Table 1). Nevertheless, the temporal variations observed display different amplitudes and profiles of expression with respect to patterns described in arrested cells (Supplementary Fig. 1b). The amplitude for *Per1* transcripts varied 7-fold over time in arrested cells and only 1.5-fold under proliferation. *Rev-erbα* reached 5- and 4-fold increases in arrested and proliferative cells, respectively. In addition, synchronized proliferating cells displayed a significant daily rhythm in levels of PER1-

Table 1 Periodic analysis by COSINOR/RAIN correlation of gene expression and metabolic parameters under both growth conditions (arrest and proliferation)

Growth condition						
	Partial arrest			Proliferative		
	p value	Acrophase (h)	Period (h)	*p* value	Acrophase (h)	Period (h)
1- Molecular level						
a. mRNA expression						
Per1	**0.0012**[b]	**20**	**28**	*0.0256*[a,c]	4	16
Rev-erb α	*0.0461*[a]	*16*	*24*	ns[b]		
ChoK α	**0.0045**[b]	**16–20, 48**	**32**	ns[b]		
Pcyt-2	*0.0329*[a, c]	*12, 28*	*16*	ns[b]		
2- Metabolic level						
a. Total GPLs	**0.0159**[a]	**0**	**20**	*0.036*[a]	*20*	*24*
b. Individual GPLs	**cpm**			**pix**		
PC	ns[a]			*0.03*[a]	*24*	*32*
PE	**0.006**[b]	**8**	**32**	*0.036*[a, c]	*12*	*32*
PC/PE	**0.008**[a]	**4, 32**	**28**	*0.025*[a, c]	*28*	*32*
c. Enzymatic activities						
Total PAP	**0.0308**[a]	**24**	**30**	**0.0277**[a, c]	**0**	**24**
LPAAT	ns[a]			ns[a]		
LPCAT	ns[b]			ns[a]		
LPEAT	ns[a]			ns[a]		
d. Redox state						
WT	**0.001**[a]	**0**	**12**	**0.0071**[a, c]	**0**	**12**
E1	Non-determined			**0.0185**[a]	**6**	**18**
e. PRX expression SO_3	**0.038**[b]	**6**	**24**	**0.005**[b]	**30**	**30**
f. Endogenous GPLs content						
PC	Non-determined			ns[a]		
PE				**0.0264**[b]	**6**	**24**
PC/PE				*0.0323*[a, c]	*12*	*24*
g. BOR	Non-determined			**0.0109**[a, c]	**0–6**	**30**

Statistical analysis was performed with results from 3/5 independent samples for each time in T98G cell grown under arrest or proliferative conditions. To test the time effect in the relative RNA expression or metabolic aspects, a periodic adjustment model—COSINOR—was applied for each data set examined as described in "Materials and Methods." When the model assumptions were infringed, the RAIN analysis was used. The COSINOR analysis includes r^2, acrophase, and period. Acrophase denotes the time at which the variable reaches the maximum observed value; the analysis considered a period from 12 to 30 h and significance at $p < 0.05$ (values in bold). Significant periodic effects of time by RAIN or COSINOR periodic model better than linear model according AIC are in bold. Significant periodic effects of time by COSINOR, but where the whole model does not perform better than null linear model (according AIC) are set in italics

ns, non-significant

[a] COSINOR

[b] RAIN

[c] Log-transformed variable

like protein by immunocytochemistry (ICC) ($p < 0.005$ by analysis of variance (ANOVA)) (Fig. 1a–c), with highest levels at 18 and 24 h after synchronization, differing from those at 6 and 12 h. In proliferating T98G cells after transfection with PX459-*Bmal1* plasmid (T98G E1), levels of *Per1* mRNA and protein were substantially reduced and no time related differences were seen in PER1-like protein along the 24 h examined (Fig. 1b, c).

Temporal Regulation of GPL Labeling in T98G Cells

In order to investigate the circadian regulation of cellular metabolism in T98G cells, we examined GPL labeling with ^{3}H-glycerol or ^{32}P-orthophosphate for 90 min in tumor cells previously synchronized with DEX and maintained in an arrested state or under proliferation for 48 h, at different times after synchronization.

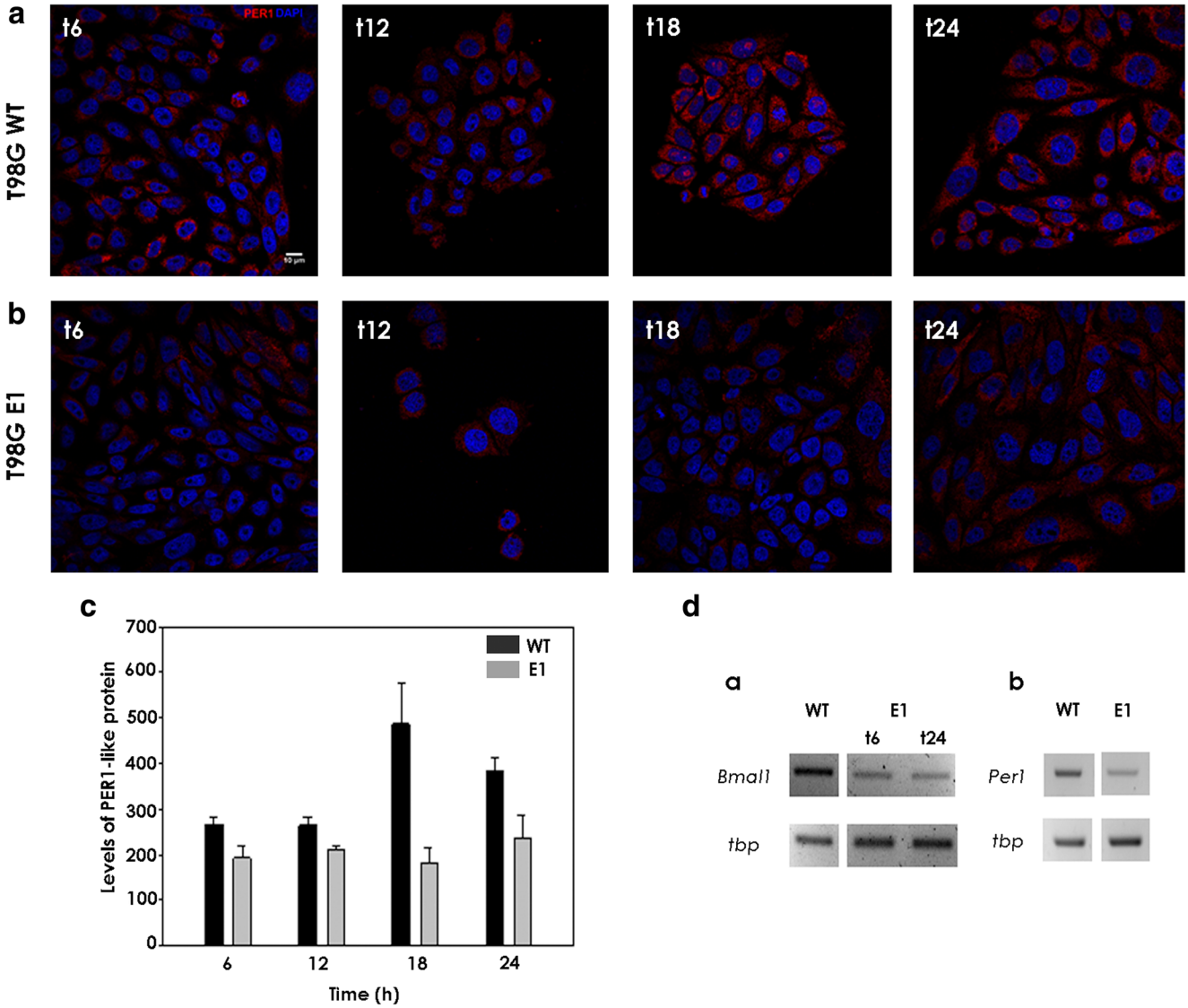

Fig. 1 Immunocytochemistry of PER1-like protein for proliferating T98G WT and E1 cell cultures after synchronization. **a**, **b** WT (**a**) or transfected cells with PX459-*Bmal1* plasmid (T98GE1 cells) (**b**) kept in the presence of serum were synchronized with a shock of 100 nM DEX for 20 min and collected at different times from 0 to 24 h. Cultures were immunolabeled with specific primary antibody for PER1-like protein (red) and with DAPI (blue) for nuclear localization and visualized by confocal microscopy as described in "Materials and Methods." Scale bar = 10 μm. **c** Histograms indicating relative levels of PER1-like protein in T98G WT cells (black) or T98G E1 cells (gray) at different times after synchronization. Data are mean ± SE. Results revealed a significant temporal variation in levels of PER1-like protein by immunocytochemistry ($p < 0.005$ by ANOVA) in WT cells, with highest levels at 18 and 24 h after synchronization, differing from those at 6 and 12 h. By contrast, T98GE1 cells under the same conditions exhibited lower immunoreactivity associated with PER1-like protein over time and no significant temporal effect at times examined. **d** RT-PCR for *Bmal1* (**a**) and *Per1* (**b**) (a downstream target gene for *Bmal1)* and the housekeeping gene *tbp* in T98GWT and T98GE1 cells. Results showed a significant decrease in both transcripts in T98G E1 glial cells. See text for further details

T98G cells totally failed to uptake ^{3}H-glycerol, irrespective of the proliferative condition examined or time of labeling as compared with positive controls (NIH3T3 fibroblasts) [3]. However, when ^{32}P-phosphate was used as a general precursor for GPL synthesis, we found a significant temporal variation in the labeling of total GPLs of arrested cells collected at different times, with highest levels at 0, 16–20, and 32–44 h after DEX synchronization and lowest levels of labeling at 8, 24, and 28 h with a period of 20 h ($p < 0.016$) (Fig. 2a (a); Table 1). When cells were maintained in FBS medium after DEX synchronization, a significant temporal variation was also observed in GPL labeling with highest levels at 0–4 and 16–24 h and lowest levels at 8 and 28–32 h (Fig. 2a (b)). Under this condition, the oscillation in metabolic GPL labeling displayed a circadian period ~ 24 h ($p < 0.036$) (Table 1).

When PC and PE labeling and the PC/PE ratio were assessed separately, a significant temporal variation was observed in arrested cells (Fig. 2b) with higher levels of

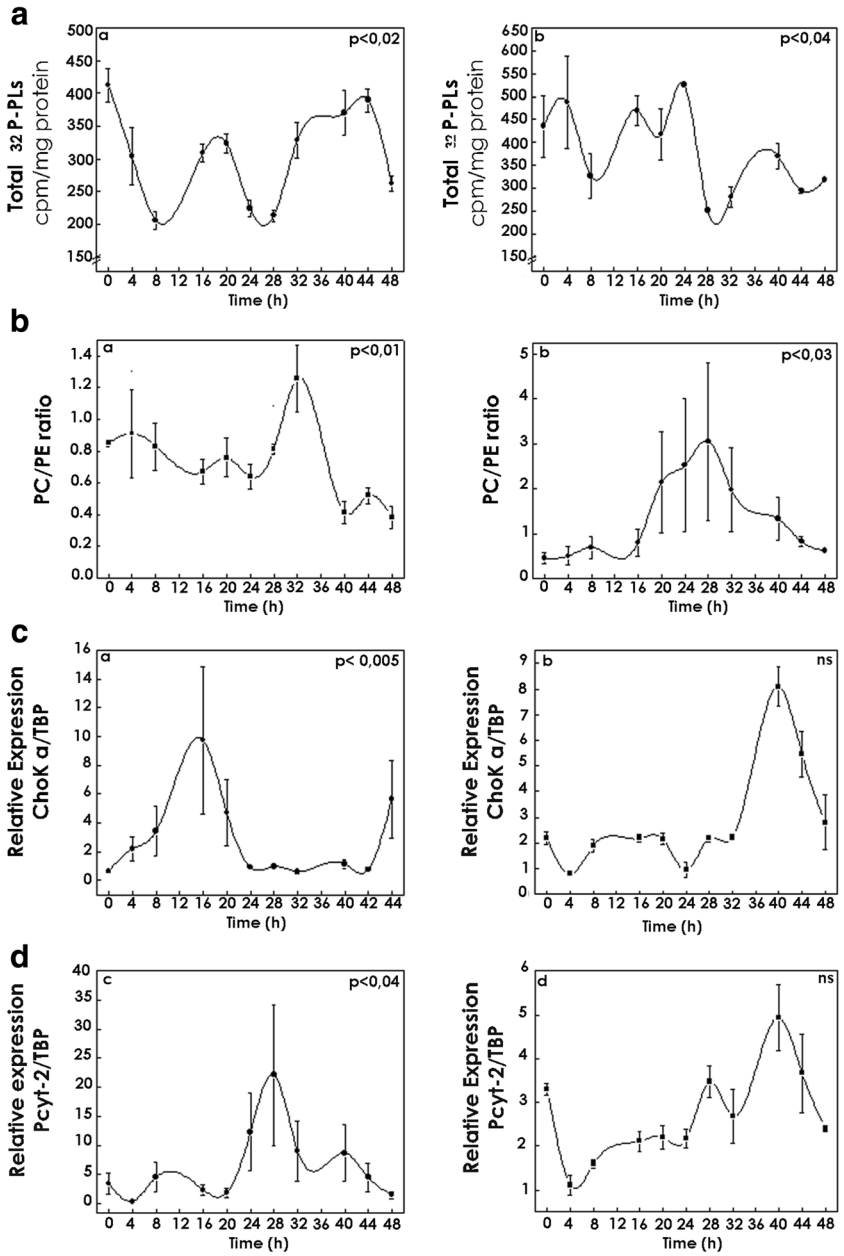

Fig. 2 **a** Temporal variations in total ^{32}P-GPL labeling in cultures of T98G cells. Cells were kept in serum-free DMEM (arrest, **a**, left panels) or in the presence of serum (proliferation, **b**, right panels) and synchronized with a shock of 100 nM DEX for 20 min and collected at different times. Cells were given a 90-min labeling pulse with ^{32}P-orthophosphate at different times after synchronization at time 0 and processed as described in "Materials and Methods." A significant time effect was found in both proliferative conditions. The COSINOR revealed a significant time effect for total ^{32}P-GPLs ($p \leq 0.05$).The results are mean ± SEM (triplicate samples from three independent experiments, $n = 3$–5/time). See text and Table 1 for further details on statistical analysis and period determination. **b** Temporal variations in ^{32}P-PC/^{32}P-PE ratio in T98G cell culture. Cells were kept in serum-free DMEM (arrest, **a**, left panels) or in the presence of serum (proliferation, **b**, right panels) and synchronized with a shock of 100 nM DEX for 20 min and collected at different times. Cells were given a 90-min labeling pulse with ^{32}P-orthophosphate at different times after synchronization at time 0. GPLs were extracted and separated by TLC as described in "Materials and Methods." A significant time effect was found in both proliferative conditions. The COSINOR/RAIN analysis revealed a significant time effect for PE and the PC/PE ratio under arrest and for PC, PE, and the PC/PE ratio under proliferation ($p \leq 0.05$). The results are mean ± SEM (triplicate samples from three independent experiments, $n = 3$–5/time). See "Materials and Methods" for further details and Table 1 for the statistical analysis and period determination. **c**, **d** Temporal variations in GPL enzyme genes *CkoKα* (**a**, **b**) and *Pcyt-2* (**c**, **d**) mRNA expression in T98G cell cultures. Cells were kept in serum-free DMEM (arrest, **a**, left panels) or in the presence of serum (proliferation, **b**, right panels) and synchronized with DEX (100 nM) for 20 min and collected at different times. *CkoKα* (**a**, **b**) and *Pcyt-2* (**c**, **d**) mRNA levels were assessed by RT-qPCR with RNA extracted from cells collected at different times during 48 h after DEX treatment at time 0; values were normalized according to the expression of the housekeeping gene TBP. A significant adjustment to a periodic function was obtained, illustrated by means of dashed lines ($p < 0.05$). The results are mean ± SEM (triplicate samples from three independent experiments, $n = 3$–5/time). See text and Table 1 for further details on statistical analysis and period determination

^{32}P incorporation into PE at 16–24 and 40–48 h and into PC at 8 h after DEX treatment (data not shown). PE labeling and the PC/PE ratio displayed a periodicity around 28–32 h ($p < 0.006$ and $p < 0.008$, respectively, Table 1). A significant variation in PC and PE labeling and in the PC/PE ratio was also observed in proliferating cells (Table 1; Fig. 2b) which as shown in Table 1 displayed a marked rhythmicity, with higher levels at 24 h and a period of 32 h for all of them ($p < 0.05$), revealing a clear temporal variation in membrane fluidity.

We further assessed the time variation in endogenous PC and PE content in proliferating cells, as shown in Supplementary Fig. 2. Although levels of PC did not vary significantly over time, PE content and the PC/PE ratio displayed a marked oscillation with a period of 24 h ($p < 0.03$) (Table 1). Pairwise comparisons revealed that PE levels at 0 and 12 h differ from those at the peak (30 h) while for PC, levels at 12 h were significantly lower than those at the peak (6 h). Notably, the metabolic labeling of GPLs exhibited the highest levels at 16–20 h, at which times the endogenous lipid content was minimal.

Temporal Regulation of Gene Expression for GPL Synthesizing Enzymes in T98G Cells under Different Proliferation Conditions

In order to further investigate temporal control of GPL synthesis in synchronized T98G cells maintained in an arrested state or under proliferation, we examined the expression of mRNAs encoding for two regulatory glycerophospholipid-synthesizing enzymes: *ChoKα* and *Pcyt-2* involved in PC and PE biosynthesis by Kennedy pathways, respectively (Fig. 2c, d). In arrested cells, *ChoKα* displayed a significant rhythmicity with the highest levels at 16–20 and 48 h after synchronization and a period of 32 h ($p < 0.004$, Table 1) while cells under proliferation showed delayed peaks of expression with highest levels at 40 h after DEX shock and no rhythmicity (Fig. 2c; Table 1).

Pcyt-2 mRNA also exhibited a rhythm in arrested cells, peaking at 24–28 h with a period of 16 h ($p < 0.04$) while proliferative cells showed delayed peaks between 28 and 40 h after DEX synchronization without periodicity (Fig. 2d; Table 1). The amplitude of expression for *ChoKα* varied significantly (7-fold) over time under both proliferative conditions while for *Pcyt-2,* it varied from 20-fold (arrest) to 4-fold (proliferation) over time.

Daily Variation in the Activity of Different T98G GPL Synthesizing Enzymes

We explored the possibility that the circadian changes observed in the metabolic labeling of total GPLs in synchronized T98G cells under different proliferative states were linked to similar variations in the activity of enzymes involved in the de novo synthesis of GPLs. For this, we determined the in vitro activities of PAP (total PAP, PAP1, and PAP2) and lysophospholipid acid acyltransferase (LPAAT) in homogenates of synchronized T98G cells collected every 6 h at different times ranging from 0 to 36 h under both proliferation conditions (with/without serum) (Supplementary Fig. 3; Fig. 3).

LPAAT Activity

PA, the main precursor of GPLs, is synthesized by the acylation of lysophosphatidic acid (LPA) catalyzed by LPAAT. In synchronized cells, the acylation of LPA exhibited no significant temporal variations under either condition (Supplementary Fig. 3); however, for proliferating cells, LPAAT activity peaked at 30 h and the lowest levels were seen at 18 h after synchronization. Post hoc comparisons showed that levels at 30 h differed from those from 0 to 18 h, as well as from those at 36 h.

PAP Activity

PA, precursor of all GPLs, is dephosphorylated to DAG by PAPs to synthesize PC and PE [17]. Since the activities of two PAP isozymes, PAP1 and PAP2, have been found in T98G homogenates, we assessed total and individual PAP activities. PAP1 is primarily involved in lipid synthesis in the endoplasmic reticulum and PAP2 is mainly involved in membrane lipid signaling.

In both conditions, total PAP activity displayed a temporal oscillation with a period between 24 (proliferation) and 30 h (arrest) (Fig. 3; Table 1) ($p < 0.03$). The highest levels of activity were found in arrested cells at 18, 24, and 30 h and the lowest at 12 h; post hoc comparisons showed that levels at 30 h differed from those at 12 h (Fig. 3a). In the case of proliferating T98G cells, activity levels peaked mainly at 24 h after synchronization and post hoc comparisons showed that these levels differed from those at 12 h (Fig. 3b). This oscillation exhibited a period of 24 h ($p < 0.03$) (Table 1). In arrested cells, both PAP1 and PAP2 activities were detected in T98G preparations but no significant variations were found over time.

Temporal Contribution of the Different LPLAT Activities to GPL Remodeling in Arrested and Proliferating T98G Cells

To investigate whether the remodeling of GPLs varies across time, we assessed the activity of LPLATs involved in the reacylation of other lysophospholipids (Lands Cycle) in arrested and proliferating T98G cells after DEX synchronization. We found slight temporal variations in the activity of LPLATs for the different GPLs examined in both conditions tested (Supplementary Fig. 3). In arrested cells,

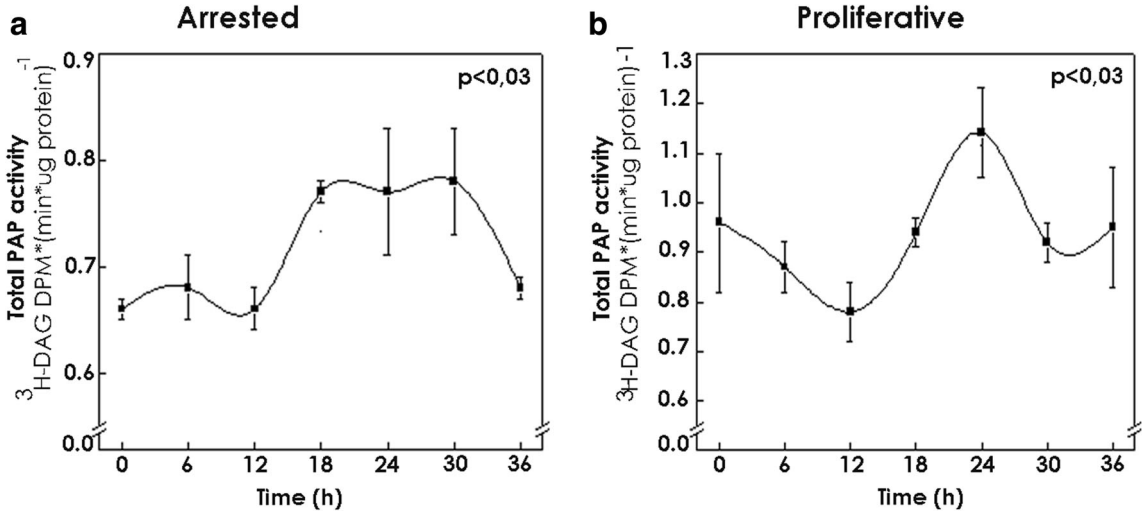

Fig. 3 Temporal variations in total PAP activity in cultures of T98G cells. Cells were kept in serum-free DMEM (arrest, **a**, left panel) or in the presence of serum (proliferation, **b**, right panel) and synchronized with a shock of 100 nM DEX for 20 min and collected at different times. The activity of total phosphatidate phosphohydrolase (PAP) was determined in cultures collected at different times after DEX synchronization as described in "Materials and Methods." The COSINOR analysis reveals a significant time effect on enzyme activity ($p < 0.03$) in both proliferative conditions. Results are the mean ± SEM of two independent experiments ($n = 4$/group). See text for further details and Table 1 for the statistical analysis and period determination

lysophosphatidylcholine acyltransferase (LPCAT) displayed a profile of activity with the highest levels at 18, 30, and 36 h ($p < 0.015$ by ANOVA); post hoc comparisons showed that levels at 36 h differed from those at 0, 12 and 24 h and levels at 30 h differed from those at 12 h post synchronization. Lysophosphatidylethanolamine acyltransferase (LPEAT) activity also exhibited a significant variation in arrested cells ($p < 0.05$ by ANOVA), with levels peaking at 30 h and differing from those at times ranging from 0 to 18 h. By contrast, no significant differences were found in activity levels for these LPLATs in proliferating cells.

Temporal Regulation of Redox Metabolism in T98G Cells

Redox State

In order to further investigate the metabolic/redox clock in these cells, the redox state was assessed in cultured T98G cells under arrest or proliferation (Fig. 4a, b). Cells were harvested at 6 h intervals after DEX synchronization during 36 h and the redox state of the cells was analyzed by incubation with 2′,7′-dichlorodihydrofluorescein diacetate (0.2 μM) for 40 min as stated in "Materials and Methods." When the fluorescence intensity was analyzed by flow cytometry, a significant temporal variation in the cellular redox state was observed in both growth conditions ($p < 0.01$ by Kruskal-Wallis) exhibiting a period of 12 h in each situation ($p < 0.008$, Table 1). In another series of studies designed to investigate the effect of the molecular clock on the redox cycles described above, the redox state was assessed in proliferating T98G cells after transfection with PX459-*Bmal1* plasmid (T98G E1) in order to knockdown *Bmal1* expression (Fig. 4c). Under this condition, the amplitude of the 12-h cycle in the redox state was substantially diminished and the 12-h rhythm extended to 18 h (Fig. 4c; Table 1).

Cycles of PRX Oxidation

In a series of experiments addressed at studying the reduction/oxidation cycles in synchronized T98G cells kept under different proliferative conditions, the oxidized/hyperoxidized PRX ($SO_{2/3}$-PRX) levels were determined by Western blot. The results indicate that oxidized/hyperoxidized PRX displays a significant temporal variation in both growth conditions ($p < 0.05$ by Kruskal-Wallis) (Fig. 5) with a period of about 24 h (arrested cells, $p < 0.04$) or 30 h (proliferative cells, $p < 0.005$) (Table 1). In arrested cells, $SO_{2/3}$-PRX levels were higher at 24–30 and 48 h whereas under proliferation, oxidized/hyperoxidized PRX levels exhibited higher levels at 12 and at 24–30 and 48 h.

Differential Time Response of Cell Viability to Bortezomib Treatment

When T98G cells grown under proliferation were treated with Bortezomib (500 nM) after DEX synchronization and their viability compared with vehicle-treated controls, we found a significant temporal effect of the drug treatment, with the lowest levels of viability in a time window ranging between 12 and 24 h (Fig. 6). The statistical analysis clearly shows a significant effect of time, treatment, and interaction ($p <$

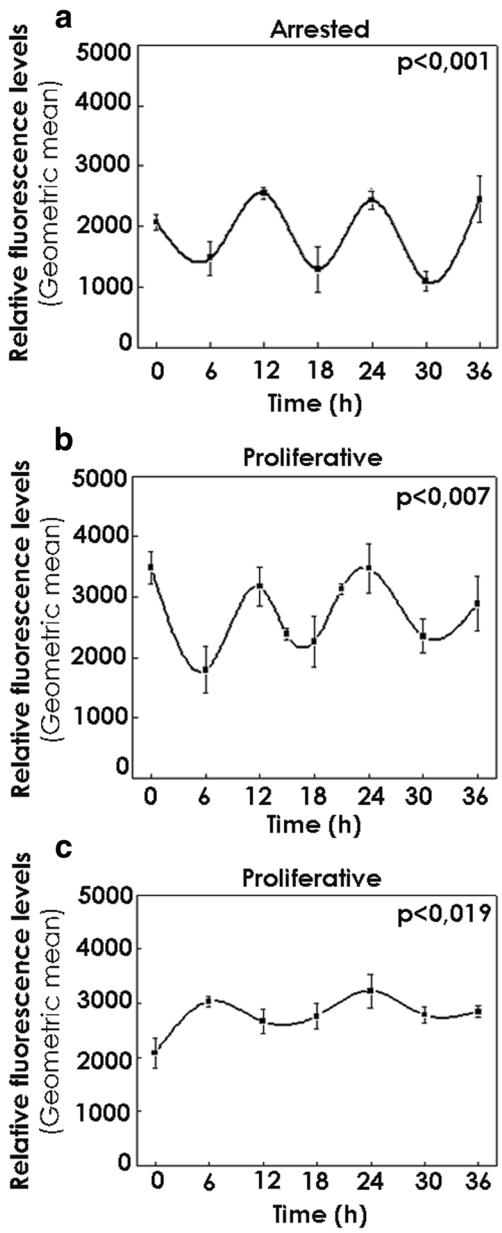

◀ **Fig. 4** Temporal variations in ROS levels in cultures of T98G cells. Cells were kept in serum-free DMEM (arrest, **a**, top panel) or in the presence of serum (proliferation, **b**, **c**, middle and bottom panels) and synchronized with a shock of 100 nM DEX for 20 min and collected at different times. Cells were harvested at 7-h intervals after DEX synchronization during 36 h, and the redox state of the cells was analyzed with the fluorescent probe 2′,7′-dichlorodihydrofluorescein diacetate to a final concentration of 0.2 μM as described in "Materials and Methods." Cells were washed twice with PBS 1×, and the fluorescence intensity was analyzed by flow cytometry. A significant temporal variation was observed in T98G WT cells (arrest, **a**, top panel; proliferation, **b**, middle panel) under both growth conditions ($p < 0.05$ by Kruskal-Wallis) with a period of 12 h ($p < 0.05$). **c** Cells kept in the presence of serum were transfected with PX459-*Bmal1*plasmid (T98G E1 cells), synchronized with a shock of 100 nM DEX for 20 min, collected at different times, and the redox state of the cells assessed as described above. Under this condition, the amplitude of the 12-h cycle in the redox state was substantially diminished and the 12-h rhythm extended to 18 h. The results are mean ± SEM of three independent experiments ($n = 3/5$ times). See text for further details and Table 1 for the statistical analysis and period determination

0.0001 by ANOVA) with maximal viability levels at 6 and 30 h after synchronization, differing from all other times examined. The COSINOR analysis revealed that the observed oscillation presented a period of 30 h ($p < 0.01$) (Table 1). Furthermore, to ascertain whether the molecular clock had any effect on the differential responses to bortezomib treatment, cell viability was assessed in proliferating T98G cells after transfection with PX459-*Bmal1* plasmid (T98G E1) (Fig. 6). Under this condition, the temporal responses in terms of T98G E1 cell viability to bortezomib treatment were substantially affected as compared with control cells expressing BMAL1. Although the temporal variation and its amplitude were not altered in transfected cells ($p < 0.0013$ by Kruskal-Wallis analysis), the oscillation exhibited a marked 6-h-phase advance with lowest levels of cell viability at 6 and 12 h post-synchronization

Discussion

The circadian clock operating in immortalized cells can be synchronized by multiple signaling pathways including medium exchange, trophic factors, serum, forskolin, heat shock, and glucocorticoids, all of which elicit gene expression rhythmicity [1, 34]. Confluent NIH3T3 fibroblasts synchronized by a 2-h serum shock were shown to display temporal oscillation in the expression of the clock gene *Per1* mRNA and protein, in clear antiphase to the oscillation of GPL metabolic labeling, mainly of PC, which was subject to complex temporal control involving concerted changes in the expression and/or activities of specific synthesizing enzymes [3, 4, 27, 32]. This and other reports clearly demonstrate a very tight link and cross-talk between the molecular circadian clock and lipid metabolism [3, 4, 7, 32], reviewed by [11, 35].

Disruption of the biological clock can lead to diverse pathologies; however, little is known about the temporal regulation of cellular metabolisms in tumor cells. Glioblastoma multiforme (GBM) is the most aggressive brain tumor and human glioma T98G cells constitute a very useful model to investigate the tumor-intrinsic circadian clock. To this end, we first optimized a protocol to obtain quiescent and proliferative T98G cells able to be synchronized by an extracellular signal, DEX, which has been shown to enhance circadian clock function in B16 melanoma cells and may inhibit tumor growth [36]. DEX is commonly used in patients suffering GBM, to reduce inflammation or as a chemotherapy adjuvant. With the

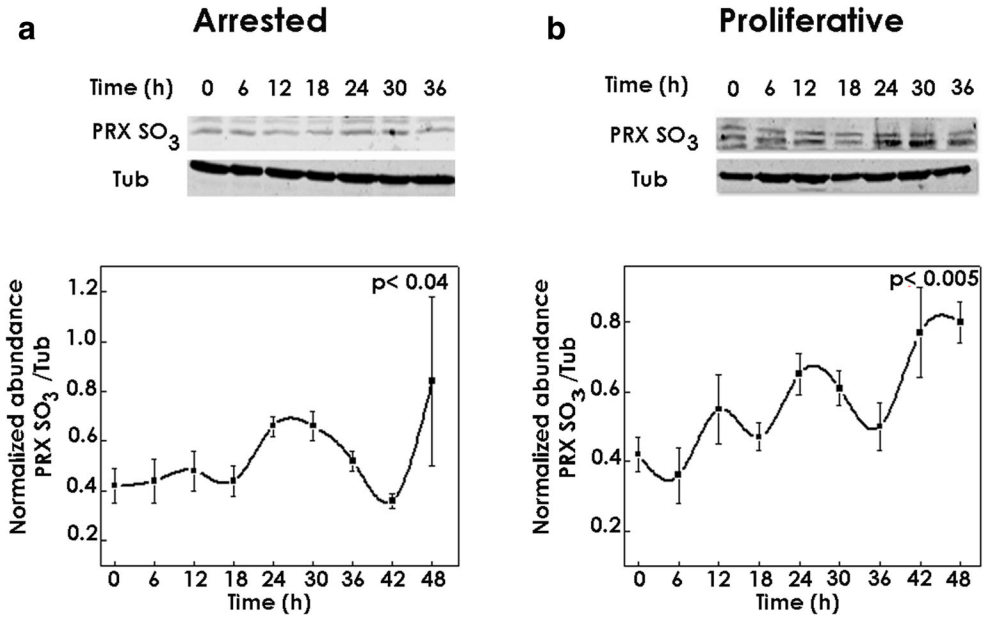

Fig. 5 Temporal variations in oxidized peroxiredoxins ($SO_{2/3}$-PRX) cycles in cultures of T98G cells. Cells were kept in serum-free DMEM (arrest, **a**, left panel) or in the presence of serum (proliferation, **b**, right panel) and synchronized with a shock of 100 nM DEX for 20 min and collected at different times. T98G cells were cultured under arrest or proliferation and harvested at 7-h intervals after dexamethasone (DEX) synchronization during 36 h in a radio-immunoprecipitation assay (RIPA) buffer containing protease inhibitor as described in "Materials and Methods." Fifty micrograms of protein were separated by SDS gel electrophoresis on 12% polyacrylamide gels. $SO_{2/3}$-PRX (ab 16,830) primary antibody was used. A significant temporal variation was observed in both growth conditions ($p < 0.05$ by Kruskal-Wallis) with a period of 24 and 30 h for arrest or proliferation, respectively ($p < 0.05$ by RAIN analysis). The results are mean ± SEM of three independent experiments ($n = 3/5$ times). See text for further details and Table 1 for the statistical analysis and period determination

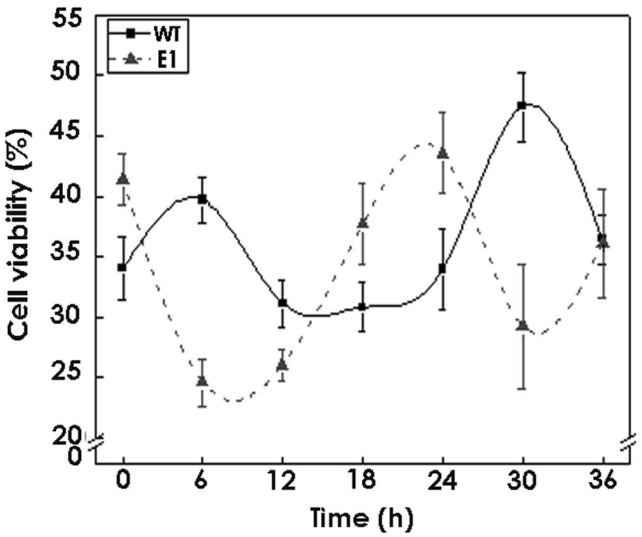

Fig. 6 Cell susceptibility to bortezomib treatment in cultures of T98G cells under proliferation. Cells were synchronized with dexamethasone (DEX, 100 nM), and bortezomib was added to a final concentration of 500 nM at different times for 36 h. Cell viability was analyzed by MTT assay as described in "Materials and Methods." A significant temporal variation was observed in levels of T98G WT (black) cell viability ($p < 0.0007$ by Kruskal-Wallis) with a period of 30 h ($p < 0.011$); in T98G E1 cells with *Bmal1* knock-down, an oscillation was also seen but exhibited a marked 6 h phase advance in cell viability (gray) ($p < 0.0013$ by Kruskal-Wallis). The results are mean ± SEM of three independent experiments ($n = 5$–6/times). See text for further details and Table 1 for the statistical analysis and period determination

protocols applied in culture, we were able to investigate the function of both the circadian molecular clock and the metabolic/redox clock [14, 35, 37, 38] in arrested and proliferating cells in an attempt to mimic two different growing/invasive conditions present in tumor cells. Proliferating cells at time 0 with no DEX treatment exhibited the highest percentage of cells under division at phase $S + G_2/M$ (>65%) and the lowest percentage arrested at G_o/G_1 (< 30%) as compared with DEX-treated cells over time (Supplementary Fig. 1). These observations clearly indicate that glucocorticoids can inhibit cancer cell proliferation by limiting the number of cells in phase S and additionally increasing the time spent in the G_1 phase (Supplementary Fig. 1) [36].

It is noteworthy that for arrested T98G cells, the circadian molecular clock controlling the rhythmic expression of clock genes *Per1 and Rev-erbα* was found to work with a period around 24–28 h (Supplementary Fig. 1; Table 1), while for the clock-controlled genes *ChoKα* and *Pcyt-2* involved in GPL synthesis, the periods were 32 and 16 h, respectively (Fig. 2; Table 1). For most genes evaluated, the peak of expression occurred at 16–24 h after synchronization. Also, under these conditions, the metabolic labeling of total GPLs and for the most abundant GPLs, PC and PE, as well as the ratio of PC to PE, exhibited daily rhythmicity from 20 to 32 h (Fig. 2; Table 1). By contrast, under proliferation, synchronized T98G cells lost their rhythmicity in the gene

expression of clock and clock-controlled genes or the oscillation period was found to be shortened (Table 1), as also shown in the expression of *Per1* and *Per2* in glioma tissue [39]. ProliferativeT98G cells nevertheless maintained the daily oscillation in the labeling of total GPLs, PC and other lipids (data not shown), as well as in the PC/PE ratio with a circadian period close to 24 h or longer (Fig. 2; Table 1) This likely reflects important temporal changes over time in membrane properties (integrity, fluidity, curvature) and in the biogenesis of new membranes for mitotic cells. The fluctuations in GPL labeling were accompanied in both conditions by concerted changes in the total activity of PAP, which provides DAG for the synthesis of more complex GPLs (PC, PE, TAG) peaking at 24 h (Fig. 3). Physiological functions affected by PAP activities include not only GPLs synthesis but also lipid signal transduction, gene expression regulation, nuclear/endoplasmic reticulum membrane growth, lipid droplet formation, and vacuole homeostasis and fusion [40–43], reviewed in [44]. In this context, a sequential but slight increase in the activity of the acyltransferases (LPAAT) was observed at 30 h to further provide PA as PAP substrate; moreover, the activity of the other acyltransferases (Lands Cycle) peaked at different times after synchronization mainly in arrested cells: LPEAT increased at 6 and 24 h and LPCAT at 12 h (Supplementary Fig. 3). These observations suggest that under arrest, a time variation in the remodeling processes of membrane GPLs is required whereas under proliferation such temporally regulated events are no longer necessary; instead, the formation of new membranes is prioritized for cell division, as observed for the metabolic labeling of total and individual GPLs, the PC/PE ratio and PAP activity. Another consequence of the lack of temporal regulation in GPL remodeling could be a shift in the membrane repair mechanism, in turn affecting physicochemical membrane properties in proliferative cells [20]. It is to be noted that the generation of LPA is mainly the result of the esterification of glycerol-3-phosphate in the de novo Kennedy pathway whereas other lysophospholipids are formed by the action of PLA activities as part of the deacylation-reacylation cycle [19]. Taking this into consideration, the possibility of a differential temporal regulation of PLA in these cells cannot be discarded. The increase in reactive oxygen species (ROS) observed in T98G cells under proliferative conditions (Fig. 4) could also be associated with changes in the Lands cycle. In this respect, previous reports have shown that increased oxidant levels were able to trigger PLA activation and to modulate GPLs acylation pathways in retina and neurons [45, 46]. Some PRX isoforms have been shown to possess PLA activities and also to be involved in membrane repair during oxidative stress conditions [47]. Based on the results presented here, we cannot rule out the possibility that PRX expression is associated with PLA activity and thus with the modulation of deacylation/re-acylation cycles.

Overall, our findings indicate that the canonical circadian molecular clock controlling rhythms in gene expression appears to shorten the oscillation period whereas the metabolic clock continues to function with a similar period to that reported under arrest, in fine tuning with cell division (see Fig. 7). In addition, a circadian metabolic rhythm has recently been reported in normal quiescent fibroblasts [48] in which the amplitude of circadian gene expression was also affected under redox stress or metabolic inhibition.

It is now known that the oxidation-reduction cycles of PRX proteins constitute a universal marker for circadian rhythms in

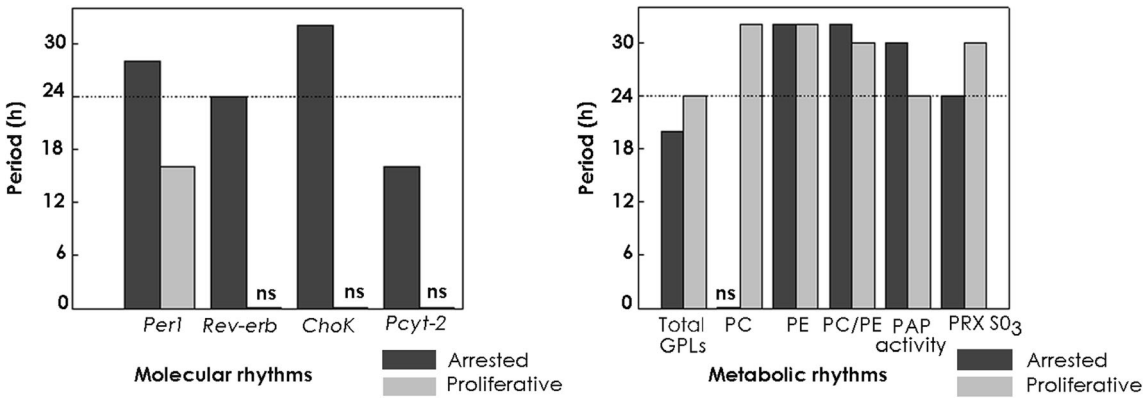

Fig. 7 Periods of molecular or metabolic rhythms in T98G cell cultures. Cells were kept in serum-free DMEM (arrest) (black bars) or in the presence of serum (proliferation) (gray bars) after synchronization with a shock of 100 nM DEX for 20 min and collected at different times along 36–48 h. Periods in hours are shown for rhythms in mRNA expression of *Per1*, *Rev-erbα*, *Chok*, and *Pcyt2* (molecular rhythms, left panel) or for metabolic rhythms in labeling of total GPLs (total GPLs), of PC, of PE, PC/PE ratio, PAP activity, and PRX-SO_3 (metabolic rhythms, right panel). For the periodic analysis, a COSINOR analysis was performed, and when the model assumptions were infringed, the RAIN analysis was applied as described in the text. The analysis considered a period (τ) ranging from 12 to 32 h and significance at $p < 0.05$. See Table 1 and text for further details

cells from humans, flies, fungus, bacteria, and archaea, likely reflecting a tight temporal control in response to environmental oxidative changes by promoting an endogenous oscillation in the generation of ROS. This mechanism, highly conserved through evolution, may confer the ability to survive cycles of oxidative stress [14, 15]. PRXs, having peroxidase activity, are mainly involved in the removal of ROS. In tumor T98G cells, significant cycles in the redox state (ROS levels) and in the abundance of oxidized/hyperoxidized PRX were clearly observed under both proliferative conditions examined, mainly displaying a bimodal rhythmicity with a 12-h period for ROS levels (Fig. 4); this observation agrees with a recent report supporting the idea that a cell-autonomous mammalian 12-h-clock distinct from the circadian clock coordinates metabolic and stress rhythms [49]. In the case of oxidized/hyperoxidized PRX cycles, the period extends from 24 h under arrest to 30 h under proliferation (Fig. 5; Table 1). Thus, at times of low ROS content (6 and 18 h after synchronization), levels of oxidized/hyperoxidized PRX were also lower and when ROS levels were high at 24 h, PRX levels were also high. Under proliferation, the overall levels of ROS are higher than in cells under arrest; nevertheless, the cell may have other antioxidant enzymes and molecules cooperating to detoxify ROS at times when ROS levels are elevated [14, 15]. Moreover, PRX cycles can persist even in the absence of the transcriptional cycles required to coordinate the circadian molecular clock [14, 15]. In this respect, our observations for the proliferating condition clearly demonstrate that even when the rhythmicity for expression of clock and clock-controlled genes was lost, the metabolic oscillator driving GPL metabolism, the redox state, and PRX cycles still operated with periods ranging from 12 to 24 h or longer. This remaining oscillatory capacity may allow tumor cells to be selectively treated with higher sensitivity at precise times using the chemotherapeutic agent bortezomib, as shown in Fig. 6. With this procedure, the highest levels of cell death (70%) are achieved from 12 up to 24 h after DEX synchronization compared with only ~ 50% cell death at other times. In this connection, daily rhythms of bioluminescence in Bmal1-luciferase expression were recently shown to occur in human and mouse GBM cells kept in culture and a circadian time-dependent sensitivity to treatment with the DNA alkylator temozolamide, a commonly used chemotherapeutic in GBM, was reported [50]. The drug effect on cell growth inhibition was found to be higher near the Bmal1/Luc peak of expression while increased sensitivity to *x*-irradiation was observed in glioma tumors when *Per1* and *Per2* expression was high [39].

Based on our observations, the intrinsic tumor cell clock can be said to consist of the canonical transcriptional clock and metabolic oscillator ticking rhythms (from 12 to 32 h) working in unison mainly under ex vivo arrest conditions or in a presumably more independent and dissociated manner in proliferating cells. In this connection, intense cross-talk has been reported between the two oscillators as seen for the $PRX_{SO2/3}$ cycles in circadian clock mutants displaying an altered circadian phase relative to wild type [14]. Here, we further investigated the interaction between the two oscillators in tumor cells, evaluating the effect of the canonical transcriptional clock alteration by knocked-down *Bmal1* on cellular processes in proliferating cells. In fact, cells transfected with the PX459-*Bmal1* plasmid exhibited a higher percentage of arrested cells (77% in G_0/G_1 phases) than in controls, decreased mRNA and protein levels for the target clock gene *Per1* and loss of PER1-like protein time variation (Fig. 1; Supplementary Fig. 1). Moreover, under this condition, the amplitude of the 12-h cycle in the redox state was substantially diminished and the rhythm extended to 18 h period (Fig. 4) while the circadian responses in cell viability to bortezomib treatment exhibited a marked 6-h-phase advance (Fig. 6).

In summary, our observations allow us to establish some degree of correlation among cell state, redox balance and GPL metabolism: under proliferation, synchronized cells experienced the highest susceptibility to the chemotherapeutic agent Bortezomib at a temporal window beginning around 12 h at which the redox state was high but GPL metabolism (endogenous levels, ^{32}P-labeling together with total PAP and some LPLATs activities) was low. The proteasome inhibitor bortezomib was shown to promote ROS generation in mitochondria of different cancer cells and ultimately to cause apoptosis [51]; these observations further support our results showing that the highest cell susceptibility to bortezomib treatment was found when the peak in ROS was attained.

Conclusions

Our findings reveal that tumor T98G cells contain an intrinsic cellular clock that regulates several cellular and metabolic functions. GBM cells were able to be synchronized by DEX and to retain the oscillatory condition under proliferation. Moreover, even when cells lost their rhythmicity in the expression of clock and clock-controlled genes or when the period of oscillation was shortened under proliferation, they still continued to oscillate for a number of metabolic/redox activities such as GPL biosynthesis, GPL enzyme activities, redox state, and PRX cycles with a similar periodicity to that under arrest (see Fig. 7). This rhythmic capacity provides an opportunity to improve chemotherapeutic treatment at precise times after cell synchronization and thereby significantly increase cell death above the average of 50%. Owing to the fact that a disruption of the molecular clock can disturb redox rhythms and differential temporal cell susceptibility to chemotherapy treatment, we may infer that cross-talk between the oscillators takes place in tumor cells to ensure tumor growth and survival over time. Furthermore, regardless of the precise nature of the

link between them, molecular and metabolic oscillators work in unison to maintain cellular homeostasis.

Materials and Methods

Materials

All reagents were of analytical grade. [^{32}P]-Na_2 orthophosphate (specific activity 285.5 Ci/mg),[2-^{3}H]-glycerol and [^{3}H]-oleic acid (9.20 Ci/mmol) were purchased from NEN Life Science Products (Boston, MA, USA). Alugram SIL G/UV_{254} TLC silica gel 60-precoated sheets were from Macherey-Nagel (Duren, Germany). GPL standards, $MgCl_2$, and ATP were from Sigma (St. Louis, MO, USA).

T98G Cell Cultures

T98G cells (ATCC, cat. No. CRl-1690, RRUD: CVCL-0556, Manassas, VA, USA) tested positive for glial cell markers and negative for mycoplasma contamination. Cells were grown in DMEM (Gibco, BRL, Invitrogen, Carlsbad, CA, USA) supplemented with 10% FBS according to [52]. After the desired degree of confluence had been achieved in a CO_2 incubator at 37 °C for 24–48 h, cells were synchronized by a 20-min shock with 100 nM DEX and allowed to grow for another 48 h in the presence (proliferative condition) or absence (quiescent condition) of 5% FBS-DMEM. After DEX synchronization (time 0), cells were collected at 4–8-h intervals during 48 h.

Glycerophospholipid Labeling

The incorporation of [^{32}P]-orthophosphate or [^{3}H]-glycerol into GPLs of T98G cells in culture was assessed at different times from 0.5 to 48 h every 4 h. A 90-min labeling pulse of [^{32}P]-Na_2Orthophosphate (10 μCi/well) or [^{3}H]-glycerol (8.5 μCi/well) was given to cultures of each condition at different times after DEX synchronization. Cells were harvested 90 min after addition of the radioactive precursor to the cultures at the different phases assessed and processed for GPL labeling.

Determination of Radioactivity in Glycerophospholipids

The labeling of total GPLs was determined according to Guido and Caputto [29]. In brief, cell preparations washed twice with 1-mM-cold phosphate-buffered saline (PBS) were resuspended in 1 mL of water and precipitated with the same volume of 10% trichloroacetic acid (TCA) and 1% phosphotungstic acid (PTA). After centrifugation (1000 rpm, 15 min), the supernatant fraction was separated. Pellets were washed three times with 5% TCA and 0.5% PTA and once with water by successive resuspension and centrifugation. Total GPLs were extracted with chloroform:methanol (2:1, *v*/*v*) as described in [53]. Lipids were resuspended in 40 μL of chloroform:methanol (1:1, *v*/*v*) for further separation by thin-layer chromatography (TLC). Radioactivity incorporated into individual GPLs was assessed by autoradiography. The protein content in cell preparations was determined by the Bio-Rad protein assay, based on the method of Bradford [54], using bovine serum albumin as standard.

Chromatographic Separation of Individual Glycerophospholipids

Individual GPLs were separated by TLC using silica gel 60 plates previously impregnated in 1.2% H_3BO_3 (in ethanol:water 1:1, *v*/*v*) (from Macherey-Nagel; Duren, Germany). The solvent system chloroform:methanol:water:ammonium hydroxide (120:75:6:2, *v*/*v*) constituted the mobile phase [55]. The bands corresponding to labeled GPLs were scraped off the silica plate and [^{32}P]-radioactivity was quantified using a liquid scintillation counter or autoradiography. In the latter case, the signal intensities from the individual GPL bands were calculated as the ratio between the signals of one individual GPL of each sample in percent of pixels and the total pixels for each sample using the gel Analyzer software. The PC/PE ratio was calculated as the ratio between the PC and PE content of each sample irrespective of any form of normalization.

In Vitro Determination of LPLAT

Proliferating or arrested T98G cells from 100 mm dishes were collected at different times from 7 to 56 h after DEX (100 mM) shock in 1 mL of PBS, lyophilized, and resuspended in 50 μL ultrapure H_2O-containing protease inhibitors (2 μg/mL leupeptin; 1 μg/mL pepstatin; 1 μg/mL aprotinin). Cell lysates were used as a source of enzyme and endogenous lysophospholipids for determination of total LPLAT activity. The activity of LPLAT was determined as "in vitro" labeling by measuring the incorporation of [^{3}H]-oleate from[^{3}H]-oleic acid (9.20 Ci/mmol) into different endogenous lysophospholipid acceptors as described in [4, 31, 56]. Under these experimental conditions, changes in the activity assessed may reflect both changes in enzyme activity and in the content of endogenous lysophospholipids (co-substrates). For the enzyme reaction the standard incubation mixture contained 60 mM Tris–HCl, pH 7.8, 4 μM [^{3}H]-oleic acid (10^5dpm/assay), 10 mM $MgCl_2$, 10 mM ATP, 75 μM CoA, and 20 μl of cellular homogenates containing 80 μg of protein in a final volume of 80 μL. The reaction was started by the addition of radiolabeled substrate resuspended in assay buffer followed by incubation for 30 min with shaking at 37 °C and was stopped by addition of 5 mL chloroform:methanol (2:1, *v*/*v*). Blanks

were prepared using boiled cellular homogenates and incubated as described above (less than 0.5% of the activity observed in the experimental samples). The lipids were extracted according to the method of Folch [57]. The lipid extract was dried under N_2, resuspended in chloroform/methanol (2:1, *v*/*v*) and spotted on silica-gel H plates. Unlabeled phospholipids were used as standards. The chromatograms were developed by two-dimensional TLC using as system solvents chloroform:methanol:ammonia (65:25:5, *v*/*v*/*v*) for the first dimension and chloroform:acetone:methanol:acetic acid:water (30:40:10:10:4, *v*/*v*/*v*/*v*) visualized with iodine vapors. The spots corresponding to the different GPLs, phosphatidic acid (PA), PC and PE, were scraped off and radioactivity was determined by liquid scintillation.

Determination of PAP Activity

Proliferating or arrested T98G cells from 100 mm dishes were collected at different times from 7 to 56 h after synchronization in 1 mL of PBS and resuspended in 50 μL ultrapure H_2O containing protease inhibitors (2 μg/mL leupeptin; 1 μg/mL pepstatin; 1 μg/mL aprotinin). Total PAP, PAP-1 and PAP-2 activities were determined by monitoring the rate of release of 1,2-diacyl-[2-^{3}H]-glycerol (DAG) from [2-^{3}H]-phosphatidic acid (PA) as previously described by Pasquaré and Giusto [58, 59]. Total PAP activity was determined in an assay containing 50 mM Tris-maleate buffer, pH 6.5, 1 mM DTT, 1 mM EDTA and 1 mM EGTA, 0.2 mM Mg^{2+}, and 80 μg of protein from the T98G preparations in a volume of 0.2 mL. The reaction was started by adding 0.6 mM of [2-^{3}H]-phosphatidate plus 0.4 mM PC. Further incubations were carried out after pre-incubating the enzyme for 10 min with 4.2 mM NEM which inhibits PAP1 activity; this activity was labeled as PAP2 and the difference between total and PAP-2 activity was labeled as PAP1 activity. The reaction was stopped at 20 min by addition of chlorophorm:methanol (2:1, *v*/*v*). DAG was separated by gradient-thickness thin-layer chromatography on silica gel G [60] and developed with hexane:diethylether:acetic acid (35:65:1, *v*/*v*/*v*). In this system, DAG migrates to three quarters of the plate and PA and MAG stay at the origin. To separate monoacylglycerol (MAG) from PA, the chromatogram was rechromatographed up to the middle of the plate using hexane:diethylether:acetic acid (20:80:2.3, *v*/*v*/*v*) as developing solvent. Each type of PAP activity was expressed as the sum of labeled DAG plus MAG × (min × μg of protein)$^{-1}$.

Redox State

Proliferating or arrested T98G cells grown as indicated above were harvested at 7-h intervals after DEX (100 nM) synchronization during 36 h, and the redox state of the cells was analyzed by flow cytometry as described in [61]. Briefly, the growth medium was removed and the cells were washed with cold PBS 1× and harvested by trypsinization; 4×10^5 cells were resuspended in PBS 1× and incubated with 2′,7′-dichlorodihydrofluorescein diacetate at 0.2 μM final concentration for 40 min at 37 °C. The cells were washed twice with PBS 1×, and the fluorescence intensity was measured by flow cytometry at 530 nm when the sample is excited at 485 nm. A negative control including cells without the fluorescent indicator was used.

Peroxiredoxin Expression

T98G cells were cultured under partial or proliferative growth conditions as indicated; cells were harvested at 7 h intervals after DEX (100 nM) synchronization during 36 h in radioimmunoprecipitation assay (RIPA) buffer containing protease inhibitor (Sigma). Total protein content in the homogenates was determined by the Bradford method. Cell lysates were resuspended in sample buffer and heated at 90 °C for 5 min. Fifty micrograms of protein were separated by SDS gel electrophoresis on 12% polyacrylamide gels as reported by [3]. $SO_{2/3}$-PRX (ab16830, Abcam cat. No. ab16830, RRID: AB-443491; dilution 1:500) primary antibodies were incubated overnight at 4 °C, and secondary antibodies were incubated for 1 h at room temperature. Finally, the membranes were scanned using an Odyssey IR Imager (LI-COR Biosciences). Densitometry quantification of specific bands was carried out with ImageJ software.

RNA Isolation and Reverse Transcription

Total RNA was extracted from cell homogenates using TRIzol® reagent following the manufacturer's specifications (Invitrogen). The yield and purity of RNA were estimated by optical density at 260/280 nm. Two micrograms of total RNA was treated with DNAse (Promega) and utilized as a template for the cDNA synthesis reaction using MMLV reverse transcriptase (Promega) and an equimolar mix of random hexamers (Biodynamics) in a final volume of 25 μL according to the manufacturer's indications.

Real-Time PCR (qPCR)

Quantitative RT-PCR was performed using SYBR Green or TaqMan Gene Expression Assays in a Rotor Q Gene (QIAGEN). The primer/probe sequences are summarized in Supplementary Table 1. The amplification mix contained 2 μL of the cDNA, 2 μL 20× mix primer/probe or 300 nM Forward-Reverse TBP primers, and 7.5 μL of Master Mix 2× (Applied Biosystems) in a total volume of 15 μL. The cycling conditions were 10 min at 95.0 °C, and 45 cycles of 95.0 °C for 15 s, 60.0 °C for 30 s, and 72 °C for 30 s. The standard curve linearity and PCR efficiency (E) were optimized. We used the $2^{-\Delta\Delta CT}$ according to Livak and Schmittgen [62] and Larionov

et al. [63] and TBP as the reference gene [3, 64]. Each RT-PCR quantification experiment was performed at least in duplicate (TaqMan or SYBR) for each sample ($n = 2$–5/sample).

Propidium Iodide Staining and Flow Cytometry

T98G cells grown in DMEM supplemented with 10% FBS were grown for 24–48 h and then synchronized by a 20-min DEX shock. After synchronization, cells were maintained in the presence or absence of 5% FBS-DMEM and collected at different times (0, 4, 8, 16, and 24 h), washed in cold PBS buffer, and fixed with ice cold 70% ethanol for at least 24 h. Cell pellets were resuspended in 150 μL of staining solution (PBS containing 50 μg/mL propidium iodide and 10 μg RNAse A) as reported [3]. Cell cycle analysis was performed with 60,000 cells on a flow cytometer (DB Bioscience). The analysis program used was ModFit software (Verity Software House, Topsham, Maine, USA).

Knock-Down of *Bmal1* Expression in T98G Cells by CRISPR/cas9

Bmal1 expression was disrupted in transfected T98G cells using the CRISPR/Cas9 genomic editing tool as previously described [65]. Briefly, we designed single guide RNAs specifically targeting exon 2 of the human *Bmal1* gene and subcloned it into the PX459 vector (Addgene) to obtain the PX459-*Bmal1* plasmid. The primer sequence corresponding to the single guide RNA was 5′CTGGCTAGAGTGTATACGTT 3′ and the complementary sequence 5′ GACCGATCTCACATATGCAA 3′. T98G wild-type cells were transfected with Lipofectamine 2000 (Invitrogen) and selected with puromycin (2 μg/mL) for 10 days. The pool of selected T98G cells was labeled as T98G E1. The disruption of *Bmal1* gene expression was checked by RT-PCR and shown to be at least 50% lower than in the WT control (Fig. 1d). Additional effects were found on the cell cycle phases by flow cytometry (Supplementary Fig. 1c) and on the expression of the downstream target gene *Per1* by RT-PCR and immunocytochemistry (Fig. 1c, d).

Immunocytochemistry

ICC was performed as described [66]. Briefly, cultured cells were fixed for 15 min in 4% paraformaldehyde in PBS and 10 min in methanol. Coverslips were washed in PBS, treated with blocking buffer (PBS supplemented with 0.1% BSA, 0.1% Tween 20, and 0.1% glycine) and incubated overnight with the PER1 antibody (Abcam cat. No. ab3443 RRID:AB_303805, dilution 1:100). They were then rinsed in PBS and incubated with goat anti-rabbit IgG (Jackson 549 antibody 1:1000) for 1 h at room temperature (RT). Coverslips were finally washed thoroughly and visualized by confocal microscopy (FV1200; Olympus, Tokyo, Japan). Cellular nuclei were visualized by DAPI staining.

Bortezomib Treatment of Proliferating T98G Cells After Synchronization and Determination of Viability

Cells were plated in 96-well plates at a density of 1×10^4 and were allowed to attach overnight at 37 °C. Cultured cell were synchronized with DEX and then either left untreated (positive control) or treated with bortezomib at different times (h) at 500 nM final concentration for 36 h. After incubation, 10 μL of MTT reagent (5 mg/mL; Sigma) were added to each well, and plates were further incubated for 2 h at 37 °C as described [67]. Then, 100 μL of DMSO:isopropanol (1:1, *v*/*v*) was added to each well followed by incubation for a few minutes at room temperature protected from light. Samples were analyzed at a wavelength of 570 nm with a reference at 650 nm in an Epoch Microplate Spectrophotometer.

Statistics

Statistical analyses involved a one- or two-way ANOVA to test the time or drug treatment effects and Kruskal-Wallis (K-W) when the normality of residuals was infringed. Pairwise comparisons were performed by the Duncan test when appropriate. For further periodic analysis, we performed a COSINOR analysis [68], and when the model assumptions were infringed, we used the RAIN analysis [69]. The analysis considered a period (τ) ranging from 8 to 32 h, and significant at $p < 0.05$.

To determine the periodic behavior of the different variables, all of them were analyzed using linear-mixed models applying the "lme" function of the "nlme" package (Pinheiro J, Bates D, DebRoy S, Sarkar D & R Core Team 2017. nlme: Linear and Nonlinear Mixed Effects Models, R package version 3.1-131.). The experiments and their repeats were incorporated as nested random effect factors. Time was considered as a fixed effect factor, including a linear component (ZT) and a periodic component ($2 \times \pi \times (ZT - \omega) \times \tau - 1$). The linear component accounts for monotonous, non-periodic effects of time, while the periodic component accounts for the oscillations present in the variable. Parameters such as phase (ω) and period (τ) were adjusted through an optimization process comparing models using the Akaike Information Criterion (AIC). In this optimization process, the intervals included in the sampling design from 12 and up to 32 h were tested as possible periods. The phases tested correspond to the sampling design times from zero to the maximum period contemplated. Additionally, the best fitted model was compared, using the procedure described, with a null model with the same random effect factors but with only the linear component of time (ZT) as a fixed effect factor. In all cases, the assumptions of normality and homogeneity of variance of the residues were tested. The logarithmic transformation of the variables was only applied when the assumptions were not fulfilled. The proportion of the variance explained by the fixed effect factors, such

as the effect of both linear and periodic time on each variable, was estimated according to Nakagawa et al. [68, 70]. When the violation of the assumptions could not be corrected for a certain variable, they were analyzed using the RAIN algorithm [69], for which the values of the repeats were averaged, the measurements were standardized by experiment and the linear effect of time was discounted when necessary, before applying the RAIN algorithm. All analyzes were carried out in the R environment (R Core Team 2017. R: A language and environment for statistical computing, Vienna, Austria URL: https://www.r-project.org).

Acknowledgments The authors are grateful to Mrs. Susana Deza and Gabriela Schanner for their excellent technical support and to Dr. Laura Allende for the gift of the PX459-plasmid.

Author Contributions LSA**,** PMW, MEG designed research; LSA, PMW, VG, GAS, SJP performed research; MEG, SJP, GAS contribute new reagents/analytic tools; LSA**,** PMW, LDG, GAS, SJP, MEG analyzed data; MEG wrote; All authors read and approved the final manuscript.

Funding This work has been supported by Agencia Nacional de Promoción Científica y Técnica (FONCyT, PICT 2010 No. 647 and PICT 2013 No. 021), Consejo Nacional de Investigaciones Científicas y Tecnológicas de la República Argentina (CONICET) (PIP 2014), Secretaría de Ciencia y Tecnología de la Universidad Nacional de Córdoba (SeCyT-UNC), and John Simon Guggenheim Memorial Foundation for Latinoamérica and Caribe (2009) in Natural Sciences.

Compliance with Ethical Standards

Conflict of Interests The authors declare that they have no competing interests.

Abbreviations Chokα, Choline kinase α; CTP, Phosphoethanolamine cytidylyltransferase 2 (*Pcyt-2*); CCG, Clock-control gene; GPL, Glycerophospholipid; DAG, Diacylglycerol; DEX, Dexamethasone; LPLAT, Lysophospholipid acyl transferase; PC, Phosphatidylcholine and; PE, Phosphatidylethanolamine; PAP, Phosphatidate phosphohydrolase; ROS, Reactive oxygen species; ICC, Immunocytochemistry

References

1. Balsalobre A, Damiola F, Schibler U (1998) A serum shock induces circadian gene expression in mammalian tissue culture cells. Cell 93(6):929–937
2. Nagoshi E, Brown SA, Dibner C, Kornmann B, Schibler U (2005) Circadian gene expression in cultured cells. Methods Enzymol 393: 543–557
3. Acosta-Rodríguez VA, Márquez S, Salvador GA, Pasquaré SJ, Gorné LD, Garbarino-Pico E, Giusto NM, Guido ME (2013) Daily rhythms of glycerophospholipid synthesis in fibroblast cultures involve differential enzyme contributions. J Lipid Res 54(7):1798–1811
4. Gorné LD, Acosta-Rodríguez VA, Pasquaré SJ, Salvador GA, Giusto NM, Guido ME (2015) The mouse liver displays daily rhythms in the metabolism of phospholipids and in the activity of lipid synthesizing enzymes. Chronobiol Int 32(1):11–26
5. Mohawk JA, Green CB, Takahashi JS (2012) Central and peripheral circadian clocks in mammals. Annu Rev Neurosci 35:445–62
6. Lahti T, Merikanto I, Partonen T (2012) Circadian clock disruptions and the risk of cancer. Ann Med 44(8):847–853
7. Gooley JJ, Chua EC-P (2014) Diurnal regulation of lipid metabolism and applications of circadian Lipidomics. J Genet Genom 41(5):231–250
8. Hanahan D, Weinberg Robert A (2011) Hallmarks of cancer: the next generation. Cell 144(5):646–674
9. Takahashi JS, Hong H-K, Ko CH, McDearmon EL (2008) The genetics of mammalian circadian order and disorder: implications for physiology and disease. Nat Rev Genet 9(10):764–775
10. Asher G, Schibler U (2011) Crosstalk between components of circadian and metabolic cycles in mammals. Cell Metab 13(2):125–137
11. Bass J, Takahashi JS (2010) Circadian integration of metabolism and energetics. Science 330(6009):1349–1354
12. Bray MS, Young ME (2011) Regulation of fatty acid metabolism by cell autonomous circadian clocks: time to fatten up on information? J Biol Chem 286(14):11883–11889
13. Eckel-Mahan KL, Patel VR, Mohney RP, Vignola KS, Baldi P, Sassone-Corsi P (2012) Coordination of the transcriptome and metabolome by the circadian clock. Proc Natl Acad Sci U S A 109(14): 5541–5546
14. Edgar RS, Green EW, Zhao Y, van Ooijen G, Olmedo M, Qin X, Xu Y, Pan M et al (2012) Peroxiredoxins are conserved markers of circadian rhythms. Nature 485(7399):459–464
15. O'Neill JS, van Ooijen G, Dixon LE, Troein C, Corellou F, Bouget F-Y, Reddy AB, Millar AJ (2011) Circadian rhythms persist without transcription in a eukaryote. Nature 469(7331):554–558
16. van Meer G, Voelker DR, Feigenson GW (2008) Membrane lipids: where they are and how they behave. Nat Rev Mol Cell Biol 9(2): 112–124
17. Hermansson M, Hokynar K, Somerharju P (2011) Mechanisms of glycerophospholipid homeostasis in mammalian cells. Prog Lipid Res 50(3):240–257
18. Kennedy EP, Weiss SB (1956) The function of cytidine coenzymes in the biosynthesis of phospholipides. J Biol Chem 222(1):193–214
19. Shindou H, Hishikawa D, Harayama T, Yuki K, Shimizu T (2009) Recent progress on acyl CoA: lysophospholipid acyltransferase research. J Lipid Res 50(Suppl):S46–S51
20. Hishikawa D, Hashidate T, Shimizu T, Shindou H (2014) Diversity and function of membrane glycerophospholipids generated by the remodeling pathway in mammalian cells. J Lipid Res 55(5):799–807
21. Li Z, Vance DE (2008) Phosphatidylcholine and choline homeostasis. J Lipid Res 49(6):1187–1194
22. Araki W, Wurtman RJ (1998) How is membrane phospholipid biosynthesis controlled in neural tissues? J Neurosci Res 51(6):667–674
23. Kent C (2005) Regulatory enzymes of phosphatidylcholine biosynthesis: a personal perspective. Biochim Biophys Acta 1733(1):53–66
24. Marcucci H, Paoletti L, Jackowski S, Banchio C (2010) Phosphatidylcholine biosynthesis during neuronal differentiation and its role in cell fate determination. J Biol Chem 285(33): 25382–25393
25. Aoyama C, Liao H, Ishidate K (2004) Structure and function of choline kinase isoforms in mammalian cells. Prog Lipid Res 43(3):266–281
26. Wu G, Vance DE (2010) Choline kinase and its function. Biochem Cell Biol 88(4):559–564
27. Gréchez-Cassiau A, Feillet C, Guérin S, Delaunay F (2015) The hepatic circadian clock regulates the choline kinase α gene through the BMAL1-REV-ERBα axis. Chronobiol Int 32(6):774–784
28. Pavlovic Z, Bakovic M (2013) Regulation of phosphatidylethanolamine homeostasis—the critical role of CTP:phosphoethanolamine cytidylyltransferase (Pcyt2). Int J Mol Sci 14(2):2529–2550

29. Guido ME, Pico EG, Caputto BL (2001) Circadian regulation of phospholipid metabolism in retinal photoreceptors and ganglion cells. J Neurochem 76(3):835–845
30. Garbarino-Pico E, Carpentieri AR, Castagnet PI, Pasquaré SJ, Giusto NM, Caputto BL, Guido ME (2004) Synthesis of retinal ganglion cell phospholipids is under control of an endogenous circadian clock: Daily variations in phospholipid-synthesizing enzyme activities. J Neurosci Res 76(5):642–652
31. Garbarino-Pico E, Valdez DJ, Contín MA, Pasquaré SJ, Castagnet PI, Giusto NM, Caputto BL, Guido ME (2005) Rhythms of glycerophospholipid synthesis in retinal inner nuclear layer cells. Neurochem Int 47(4):260–270
32. Marquez S, Crespo P, Carlini V, Garbarino-Pico E, Baler R, Caputto BL, Guido ME (2004) The metabolism of phospholipids oscillates rhythmically in cultures of fibroblasts and is regulated by the clock protein PERIOD 1. FASEB J 18:519–521
33. Fu L, Kettner NM (2013) The circadian clock in cancer development and therapy. Prog Mol Biol Transl Sci 119:221–282
34. Balsalobre A, Marcacci L, Schibler U (2000) Multiple signaling pathways elicit circadian gene expression in cultured Rat-1 fibroblasts. Curr Biol, 10(20):1291–1294.
35. Ray S, Reddy AB (2016) Cross-talk between circadian clocks, sleep-wake cycles, and metabolic networks: dispelling the darkness. Bioessays 38(4):394–405
36. Kiessling S, Beaulieu-Laroche L, Blum ID, Landgraf D, Welsh DK, Storch K-F, Labrecque N, Cermakian N (2017) Enhancing circadian clock function in cancer cells inhibits tumor growth. BMC Biol 15:13
37. Brown SA (2016) Circadian metabolism: from mechanisms to metabolomics and medicine. Trends Endocrinol Metab 27(6):415–426
38. Takahashi JS (2015) Molecular components of the circadian clock in mammals. Diabetes Obes Metab 17(0 1):6–11
39. Zhanfeng N, Yanhui L, Zhou F, Shaocai H, Guangxing L, Hechun X (2015) Circadian genes Per1 and Per2 increase radiosensitivity of glioma in vivo. Oncotarget 6(12):9951–9958
40. Giusto NM, Pasquaré SJ, Salvador GA, Castagnet PI, Roque ME, Ilincheta de Boschero MG (2000) Lipid metabolism in vertebrate retinal rod outer segments. Prog Lipid Res 39(4):315–391
41. Brindley DN (2004) Lipid phosphate phosphatases and related proteins: Signaling functions in development, cell division, and cancer. J Cell Biochem 92(5):900–912
42. Pasquaré SJ, Salvador GA, Giusto NM (2004) Phospholipase D and phosphatidate phosphohydrolase activities in rat cerebellum during aging. Lipids 39(6):553–560
43. Kok BPC, Venkatraman G, Capatos D, Brindley DN (2012) Unlike two peas in a pod: lipid phosphate phosphatases and phosphatidate phosphatases. Chem Rev 112(10):5121–5146
44. Pascual F, Carman GM (2013) Phosphatidate phosphatase, a key regulator of lipid homeostasis. Biochim Biophys Acta 1831(3):514–522
45. Rodríguez Diez G, Sánchez Campos S, Giusto NM, Salvador GA (2013) Specific roles for group V secretory PLA2 in retinal iron-induced oxidative stress. Implications for age-related macular degeneration. Exp Eye Res 113:172–181
46. Sánchez Campos S, Rodríguez Diez G, Oresti GM, Salvador GA (2015) Dopaminergic neurons respond to iron-induced oxidative stress by modulating lipid acylation and deacylation cycles. PLoS One 10(6):e0130726
47. Fisher AB (2017) Peroxiredoxin 6 in the repair of peroxidized cell membranes and cell signaling. Arch Biochem Biophys 617:68–83
48. Putker M, Crosby P, Feeney KA, Hoyle NP, Costa ASH, Gaude E, Frezza C, O'Neill JS (2018) Mammalian circadian period, but not phase and amplitude, is robust against redox and metabolic perturbations. Antioxid Redox Signal 28(7):507–520
49. Zhu B, Zhang Q, Pan Y, Mace EM, York B, Antoulas AC, Dacso CC, O'Malley BW (2017) A cell-autonomous mammalian 12 hr clock coordinates metabolic and stress rhythms. Cell Metab 25(6): 1305–1319.e1309
50. Slat EA, Sponagel J, Marpegan L, Simon T, Kfoury N, Kim A, Binz A, Herzog ED et al (2017) Cell-intrinsic, Bmal1-dependent circadian regulation of temozolomide sensitivity in glioblastoma. J Biol Rhythm 32(2):121–129
51. Vriend J, Reiter RJ (2015) The Keap1-Nrf2-antioxidant response element pathway: A review of its regulation by melatonin and the proteasome. Mol Cell Endocrinol 401:213–220
52. Portal MM, Ferrero GO, Caputto BL (2006) N-terminal c-Fos tyrosine phosphorylation regulates c-Fos//ER association and c-Fos-dependent phospholipid synthesis activation. Oncogene 26(24):3551–3558
53. Bligh EG, Dyer WJ (1959) A rapid method of total lipid extraction and purification. Can J Biochem Physiol 37(8):911–917
54. Bradford MM (1976) A rapid and sensitive method for the quantitation of microgram quantities of protein utilizing the principle of protein-dye binding. Anal Biochem 72(1):248–254
55. Fine JB, Sprecher H (1982) Unidimensional thin-layer chromatography of phospholipids on boric acid-impregnated plates. J Lipid Res 23(4):660–663
56. Castagnet PI, Giusto NM (2002) Effect of light and protein phosphorylation on photoreceptor rod outer segment acyltransferase activity. Arch Biochem Biophys 403(1):83–91
57. Folch J, Lees M, Sloane Stanley GH (1957) A simple method for the isolation and purification of total lipides from animal tissues. J Biol Chem 226(1):497–509
58. Pasquare de Garcia SJ, Giusto NM (1986) Phosphatidate phosphatase activity in isolated rod outer segment from bovine retina. Biochim Biophys Acta 875(2):195–202
59. Pasquare SJ, Giusto NM (1993) Differential properties of phosphatidate phosphohydrolase and diacylglyceride lipase activities in retinal subcellular fractions and rod outer segments. Comp Biochem Physiol B 104(1):141–148
60. Giusto NM, Bazan NG (1979) Phospholipids and acylglycerols biosynthesis and 14CO2 production from [14C]glycerol in the bovine retina: The effects of incubation time, oxygen and glucose. Exp Eye Res 29(2):155–168
61. Eruslanov E, Kusmartsev S (2010) Identification of ROS using oxidized DCFDA and flow-cytometry. In: Armstrong D (ed) Advanced protocols in oxidative stress II. Humana Press, Totowa, NJ, pp. 57–72
62. Livak KJ, Schmittgen TD (2001) Analysis of relative gene expression data using real-time quantitative PCR and the 2−ΔΔCT method. Methods 25(4):402–408
63. Larionov A, Krause A, Miller W (2005) A standard curve based method for relative real time PCR data processing. BMC Bioinformatics 6:62–62
64. Garbarino-Pico E, Niu S, Rollag MD, Strayer CA, Besharse JC, Green CB (2007) Immediate early response of the circadian polyA ribonuclease nocturnin to two extracellular stimuli. RNA 13(5):745–755
65. Ran FA, Hsu PD, Wright J, Agarwala V, Scott DA, Zhang F (2013) Genome engineering using the CRISPR-Cas9 system. Nat Protoc 8(11):2281–2308
66. Morera LP, Díaz NM, Guido ME (2016) Horizontal cells expressing melanopsin x are novel photoreceptors in the avian inner retina. Proc Natl Acad Sci U S A 113(46):13215–13220
67. Vlachostergios PJ, Hatzidaki E, Stathakis NE, Koukoulis GK, Papandreou CN (2013) Bortezomib downregulates MGMT expression in T98G glioblastoma cells. Cell Mol Neurobiol 33(3):313–318
68. Nakagawa S, Schielzeth H (2013) A general and simple method for obtaining R2 from generalized linear mixed-effects models. Methods Ecol Evol 4(2):133–142
69. Thaben PF, Westermark PO (2014) Detecting rhythms in time series with RAIN. J Biol Rhythm 29(6):391–400
70. Johnson PCD (2014) Extension of Nakagawa & Schielzeth's R2GLMM to random slopes models. Methods Ecol Evol 5(9): 944–946